Journal of The Electrochemical Society, **160** (7) G3080-G3090 (2013)
0013-4651/2013/160(7)/G3080/11/$31.00 © The Electrochemical Society

JES Focus Issue on Organic and Biological Electrochemistry

Metal-Salens As Catalysts In Electroreductive Cyclization and Electrohydrocyclization: Computational and Experimental Studies

Jessica M. Yates, Jason S. Fell, James A. Miranda,[*,z] and Benjamin F. Gherman

Department of Chemistry, California State University, Sacramento, Sacramento, California 95819-6057, USA

The use of chiral Ni(II)-salen derivatives was examined in mediated electrohydrocyclization (EHC) reactions. Cyclic voltammetry established the existence of a catalytic current. Bulk electrolysis revealed a slight change in the diastereoselectivity of the cyclizations. Density functional theory (DFT) computational studies showed that Ni(II)-salen and Zn(II)-salen were the best metal-salens for electron transfer, while Co(II)-salen and Cu(II)-salen would likely be ineffective for this purpose. Electron transfer was both considerably more thermodynamically and kinetically (whether through an inner or outer sphere pathway) favorable with Ni(II)-salen and Zn(II)-salen. Computational data also suggests Ni(II)-salen to be preferred for promoting inner sphere electron transfer, due in part to the ligand-centered reduction of Ni(II)-salen, and thus for affecting stereoselectivity in mediated EHC reactions.
 [DOI: 10.1149/2.015307jes]

Manuscript submitted February 27, 2013; revised manuscript received April 8, 2013. Published April 25, 2013. This was Paper 2086 presented at the Honolulu, Hawaii, Meeting of the Society, October 7-12, 2012. *This paper is part of the JES Focus Issue on Organic and Biological Electrochemistry*.

Electrochemistry provides a convenient tool with which electrons can be selectively introduced or removed from an organic molecule.[1] It allows for the reversal of functional group polarity and can therefore produce umpolung reactions. This allows one to couple either two electrophiles or two nucleophiles in ways in which it would be otherwise impossible to accomplish. Electroreductive cyclization (ERC) refers to those processes wherein an electron-deficient alkene is tethered to an acceptor (e.g., an aldehyde or ketone) which undergoes an electrochemically promoted reductive cyclization leading to the formation of a new sigma bond between the β-carbon of the alkene and the acceptor unit. The ERC reaction was pioneered in 1988 by Baizer, Little, and co-workers.[2] Cyclic voltammetry firmly established that the α,β-unsaturated unit corresponded to the electrophore. Cyclization generally favored the formation of the product wherein the hydroxy and (methoxycarbonyl)methyl units were *trans* to one another. Sowell, Wolin, and Little used two ERC reactions during the formal total synthesis of quadrone, an anti-cancer compound.[3] The mechanism of the ERC reaction was investigated by Leonetti, Fry, and Little.[4] Electrohydrocyclization (EHC) refers to those processes which undergo an electrochemically promoted reductive cyclization leading to the formation of a new sigma bond between the β-carbons of α, β-unsaturated esters or nitriles. Moens, Baizer, and Little reported the use of an EHC reaction as a key step in the total synthesis of the natural product 1-sterpurene.[5]

Miranda, Wade, and Little reported a variant of the ERC and EHC reaction that used catalytic Ni(II)-salen as a mediator.[6] The most significant advantage of mediated electrochemical reactions over direct electrochemical reactions is the use of a more positive potential than necessary in the direct substrate reduction, resulting in a more chemoselective reaction.[7] This is of the utmost importance in complicated molecules with many different functional groups. Operating at a more positive potential allows the reduction of one part of the molecule while leaving other functional groups untouched, avoiding the need for cost and labor intensive protecting groups. Another advantage of operating at a more positive potential during industrial scale syntheses is economics. Lower cell voltage allows for lower power usage.[8] Using catalytic Ni(II)-salen as a mediator, ERC and EHC transformations were achieved in yields ranging from 60% to 94% using either a mercury pool or environmentally preferable reticulated vitreous carbon (RVC) cathode. The mechanism of mediated ERC and EHC reactions was also studied. The authors proposed the existence of a mechanistic continuum involving an equilibrium between Ni(II)-salen and two reduced forms, one being the metal-centered species **1**, the other being ligand-centered species **2** (Figure 1). In the ERC and EHC reactions, the ligand-centered species was theorized to be the dominant form of the reduced Ni(II)-salen. There is much support for the existence of **2**. Peters discovered that the catalytic reduction of 1-iodooctane in the presence of "electrogenerated nickel(I) salen" led to the formation of products from the alkylation of one or both of the imino bonds of the salen ligand.[9] They concluded that the reactive mediator that led to the alkylated products is best described by a ligand-centered species, namely Ni(II)-salen radical anion. Density functional theory (DFT) calculations carried out by Peters on the reduced Ni(II)-salen also suggested a role for the ligand-centered species in accounting for the reactivity they observed.[10,11] In addition, reduced Ni(II)-salen radical anion displays an ESR spectrum that shows partial delocalization of spin onto the ligand.[12]

In mediated ERC, while Ni(II)-salen (reduction potential or $E_{pc} = -1.60$ V vs Ag/AgCl) is an effective electrochemical mediator, the analogous Co(II)-salen ($E_{pc} = -1.10$ V vs Ag/AgCl) fails to promote cyclization.[6] Direct ERC (unmediated) occurs at a reduction potential of −2.35 V vs. Ag/AgCl. It was concluded that the 1.25 V thermodynamic barrier was too large to allow electron transfer to occur from the reduced form of the Co(II)-salen to the substrate. Miranda and Gherman have reported a technique that sought to discover if there were other metal-salen compounds that also fall within an "electrochemical potential window" in which effective ERC would occur. Using DFT calculations to predict electron affinities and cyclic voltammetry to experimentally measure reduction potentials for a wide variety of metal-salens, the authors were able to build a "training set" and "test set" of metal-salens. The correlation between the calculated electron affinities and experimental reduction potentials built from the training set worked to accurately predict reduction potentials for the test set to a mean signed error of −16 mV and a mean unsigned error of 99 mV.[13]

In this paper, we wish to report our continuing progress in the study of the mechanism of mediated ERC and EHC reactions. We studied the reactions using a combination of computational and experimental methods. Computations are first used to investigate the

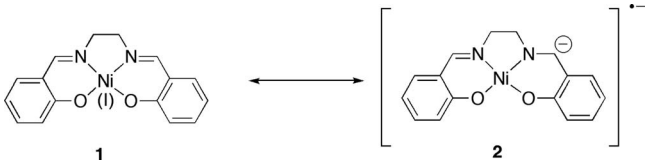

Figure 1. Reduced Ni(II)-salen (metal-centered anion vs. ligand-centered anion).

*Electrochemical Society Active Member.
[z]E-mail: miranda@csus.edu

thermodynamics, kinetics, and pathway (inner sphere versus outer sphere) of electron transfer with different metal-salens. Experimental work subsequently studied the catalytic behavior of these metal-salens by cyclic voltammetry and bulk electrolysis. It was hoped that our investigation would not only provide insight into the mediation of electron transfer by the metal-salen, but also provide an entryway into the possibility of changing the structure of the salen ligand in order to promote asymmetric EHC reactions.

Experimental

Reagents.— 1,6-hexanediol, sodium hydride (NaH) (60% oil immersion), (R,R)-(-)-*N*,*N*′-Bis(3,5-di-*tert*-butylsalicylidene)-1,2-cyclohexanediamine, and dimethyl malonate ($CH_2(CO_2Me)_2$) were purchased from Aldrich Chemical Company, Inc. Oxalyl chloride ($(COCl)_2$), (ethoxycarbonylmethylene)triphenylphosphorane, and sulfur trioxide-pyridine complex were purchased from Alfa Aesar. Deuterated chloroform ($CDCl_3$) was purchased from Cambridge Isotope Laboratories, Inc. Anhydrous dimethyl sulfoxide (DMSO), triethylamine (TEA), anhydrous tetrahydrofuran (THF), ether, hexane, absolute ethanol (abs. EtOH), and anhydrous dimethylformamide (DMF) were purchased from EMD. Potassium carbonate (K_2CO_3) and magnesium sulfate ($MgSO_4$) were purchased from Fisher Chemical. Sodium sulfate (Na_2SO_4) was purchased from J.T. Baker Chemical Co. Dichloromethane (DCM) and ethyl acetate (EtOAc) were purchased from Mallinckrodt. DCM was distilled over calcium hydride prior to use. Nickel (II) acetate and *o*-phenylenediamine were purchased from Matheson Coleman & Bell. (S,S)-(+)-*N*,*N*′-Bis(3,5-di-*tert*-butylsalicylidene)-1,2-cyclohexanediamine was purchased from Strem Chemicals. 3,5-di-*tert*-butylsalicylaldehyde, ethylenediamine, tetra-*n*-butylammonium hexafluorophosphate ($n$$Bu_4NPF_6$), and diethylphosphonoacetic acid ethyl ester were purchased from TCI Co. Unless otherwise stated, all reagents were used unpurified from the supplier. Air sensitive reactions were performed under nitrogen atmosphere and used oven-dried glassware with standard syringe/septa techniques.

Spectroscopic identification of products, cyclic voltammetry, and bulk electrolysis NMR.— ^{1}H NMR spectra were recorded using either a Bruker Avance 300 or Avance III 500 NMR at ambient temperature. ^{13}C NMR spectra were recorded using a Bruker III Avance spectrometer at 125 MHz at ambient temperature. All chemical shifts are reported in ppm relative to TMS (0.00 ppm) or $CDCl_3$ (7.27 ppm) on the δ scale. Multiplicity (br: broad, s: singlet, d: doublet, t: triplet, q: quartet, quint: quintet, m: multiplet) and coupling constants are in hertz (Hz).

IR.— A Perkin Elmer System 200 FT-IR Spectrometer was used for all IR measurements.

GC-MS.— An Agilent Technologies 7890A GC System containing an Agilent J&W GC Column (stationary phase: HP-5MS, 30 m × 0.250 mm × 0.25 μm) with a 5975C inert XL EI/CI MSD with Triple-Axis Detector was used to obtain all GC-MS data. The method used for all runs was: 40°C for 1 min, 5°C/min to 110°C, 20°C/min to 280°C, hold for 2 min.

Electrochemistry.— A BASi C-3 Cell Stand and an Electrochemical Analyzer/Workstation, model 600D, from CH Instruments were used for all electrochemical experiments.

General Procedure for Cyclic Voltammetry (CV).— A standard single compartment glass cell vial was used for CV experiments. The working electrode was a glassy carbon electrode (surface area: 7 mm^2) and a platinum electrode was used as the auxiliary electrode (surface area: 2 mm^2). The potentials were recorded against the reference of Ag/AgCl, NaCl sat., which was separated from the medium by a porous Vycor membrane (surface area: 28 mm^2). This electrode has a potential of −0.045 V versus the saturated calomel electrode (SCE) at 25°C.[14] The voltage scan rate (VSR) was varied between 0.2 V/s and 1.0 V/s. The electrodes were immersed in a quiet solution of Ni(II) salen mediators and 0.1 M $n$$Bu_4NPF_6$ in 5 mL of anhydrous DMF. The concentration of the mediator was either 1 mM or 5 mM depending upon the CV experiment. The solution was deoxygenated for at least 10 min by bubbling nitrogen in the solution and the cell contents were maintained under a nitrogen atmosphere during the experiment. CV was performed using a computer-controlled potentiostat electroanalytical system. The data was collected and exported to a spreadsheet program.

General Procedure for Bulk Electrolysis (BE): All reactions were carried out in a two compartment BE glass cell. The working electrode was a reticulated vitreous carbon (RVC) electrode (area: 31 cm^2). A coiled platinum wire (length: 23 cm) within a fritted glass isolation chamber was used as the auxiliary electrode. The reference electrode was a Ag/AgCl, NaCl sat., that was separated from the medium by a porous Vycor membrane (surface area: 28 mm^2). This electrode has a potential of −0.045 V versus the SCE at 25°C.[14] A 0.1 M solution of $n$$Bu_4NPF_6$ in 85 mL of anhydrous DMF was poured into the cell containing all three electrodes. The solution was deoxygenated for 20 min by bubbling nitrogen in the solution and the cell contents were maintained under a nitrogen atmosphere during the experiment. The solution was stirred with a stir bar throughout the entire experiment. A pre-electrolysis potential, depending upon the mediator used, was applied and the current was monitored until it leveled off. In a separate vial, a 6.55 mM solution of the EHC substrate **(3)** was prepared in a solution containing 0.1 M solution of $n$$Bu_4NPF_6$ in 5 mL of anhydrous DMF. To this solution 1 mM of the mediator and 2 equivalents of the proton donor dimethyl malonate were added. After the pre-electrolysis, the current was stopped and the solution containing the EHC substrate was added to the cell. The current flow was resumed by applying the same potential applied during the pre-electrolysis step. The reaction was monitored by GC. Once complete, the solution was transferred to a RBF and cooled to 0°C. The reaction was quenched with 60 mL of H_2O and extracted with diethyl ether (60 mL × 3). The combined organic layers were washed with brine (60 mL × 3) and dried over Na_2SO_4. The solvent was removed by rotary evaporation to give the crude BE product.

*Synthesis of [N,N′-Bis(di-salicylidene)-1,2-ethylenediamine] Nickel(II) (**4**)*.— This compound was prepared according to a published procedure.[15] ^{1}H NMR ($CDCl_3$, 500 MHz): δ 7.46 (s, 2H), 7.20 (m, 2H), 7.03 (m, 4H), 6.52 (m, 2H), 3.43 (s, 4H); IR (KBr): 2800, 1625.45, 1537.17, 1451.92, 1348.78, 1200.10, 1127.57 cm^{-1}.

*Synthesis of [(R,R)-N,N′-Bis(3,5-di-tert-butylsalicylidene)-1,2-cyclohexanediamine]Nickel(II) (**5**)*.— A 100 mL RBF was filled with (R,R)-(-)-*N*,*N*′-Bis(3,5-di-*tert*-butylsalicylidene)-1,2-cyclohexanediamine (1.000 g, 1.829 mmoles) and 45.0 mL of abs. EtOH. Ni(II) acetate (0.4552 g, 1.829 mmoles) was added to the mixture. The solution was heated to reflux for 1 h and then cooled to r.t. The solution was vacuum filtered and washed with cold EtOH. The product (1.100 g, 1.825 mmoles, 99.78% yield) was dark yellow crystals. ^{1}H NMR ($CDCl_3$, 300 MHz): δ 7.39 (s, 2H), 7.29 (d, J = 2.62 Hz, 2H), 6.87 (d, J = 2.5 Hz, 2H), 2.96 (m, 2H), 2.47 (m, 4H), 1.93 (m, 4H), 1.41 (s, 18H), 1.25 (s, 18H); IR (KBr): 2952.16, 2866.99, 1617.36, 1529.58, 1435.36, 1324.29, 1256.54, 1174.08 cm^{-1}. ^{1}H NMR data matched literature values.[16]

*Synthesis of [(S,S)-N,N′-Bis(3,5-di-tert-butylsalicylidene)-1,2-cyclohexanediamine]Nickel(II) (**6**)*.— A 100 mL RBF was filled with (S,S)-(+)-*N*,*N*′-Bis(3,5-di-*tert*-butylsalicylidene)-1,2-cyclohexanediamine (0.6082 g, 1.112 mmoles) and 45.0 mL of abs. EtOH. Ni(II) acetate (0.2731 g, 1.097 mmoles) was added to the mixture. The solution was heated to reflux for 1 h and then cooled to r.t. The solution was vacuum filtered and washed with cold EtOH. The product (0.6205 g, 1.029 mmoles, 92.54% yield) was dark yellow crystals. ^{1}H NMR ($CDCl_3$, 300 MHz): δ 7.39 (s, 2H), 7.29 (d, J = 2.6 Hz, 2H), 6.88 (d, J = 2.5 Hz, 2H), 2.95 (m, 2H), 2.43 (m, 4H), 1.91 (m, 4H), 1.41 (s, 18H), 1.25 (s, 18H); ^{13}C NMR ($CDCl_3$, 125 MHz): δ 162.69 (2CH), 157.69 (2C), 140.21 (2C), 135.81 (2C), 128.95

(2CH), 126.19 (2CH), 119.44 (2C), 69.79 (2CH), 35.81 (2C), 33.77 (2C), 31.35 ($6CH_3$), 29.65 ($6CH_3$), 28.85 ($2CH_2$), 24.47 ($2CH_2$); IR (KBr): 2952.52, 2866.54, 1615.93, 1529.74, 1435.54, 1324.71, 1256.48, 1173.90 cm^{-1}.

*Synthesis of Hexanedial (**7**).*— The general oxidation procedure of Swern was followed.[17] A 3-neck 1000 mL RBF was cooled to −78°C and filled with 700.0 mL of anhydrous DCM. Oxalyl chloride (10.00 mL, 0.1143 moles) was added to the solution and stirred for 20 min. DMSO (15.72 mL, 0.2032 moles) was added dropwise and stirred for 30 min. 1,6-hexanediol (3.000 g, 0.02539 moles) was dissolved in 5.0 mL of anhydrous DCM and added slowly. The solution was stirred for 1 h. TEA (35.39 mL, 0.2539 moles) was added and the reaction was stirred overnight. The RBF was then placed in an ice bath and the solution diluted with DCM and the reaction quenched with DI H_2O. The solution was transferred to a separatory funnel and the aqueous layer removed. The organic layer was washed with 1M HCl (500 mL × 1), DI H_2O (500 mL × 1), sat. $NaHCO_3$ (500 mL × 1), and brine (500 mL × 1). The organic layer was dried over $MgSO_4$, filtered through celite and silica, and the solvent removed by rotary evaporation. The product (2.413 g, 0.02114 moles, 79.54% yield) was a clear yellow oil. ^{1}H NMR ($CDCl_3$, 300 MHz): δ 9.78 (t, J = 1.4 Hz, 2H), 2.48 (m, 4H), 1.67 (m, 4H); ^{13}C NMR ($CDCl_3$, 125 MHz): δ 201.84 (2CH), 43.57 ($2CH_2$), 21.48 ($2CH_2$); IR (neat): 2940.40, 1719.92, 1595.76, 1439.74, 1251.89, 1053.11 cm^{-1}; MS: *m/z* 114.9, 96.1, 81.0, 72.1; R_f: 0.095 (20:80 EtOAc-hexane, visualized with vanillin stain). ^{1}H NMR, ^{13}C NMR, IR, and MS data matched literature values.[18]

*Synthesis of Deca-2,8-dienedioic acid diethyl ester (**3**).*— The general olefination procedure of Wadsworth and Emmons was followed.[19] Sodium hydride (60% oil immersion) (1.576 g, 0.03941 moles) was washed with hexane (10 mL × 3) in a 3-neck 100 mL RBF. The RBF was cooled to 0°C, placed under nitrogen gas, and 30.0 mL of anhydrous THF was added. Diethylphoshonoacetic acid ethyl ester (5.213 mL, 0.02627 moles) was slowly added and the solution stirred for 15 minutes. Hexanedial (**7**) (1.000 g, 0.008758 moles) was dissolved in 2.0 mL of anhydrous THF and slowly added to the solution. The solution stirred for 2.5 hours at r.t. The reaction was quenched with deionized H_2O (25 mL) and extracted with ethyl acetate (25 mL × 6). The combined organic layers were washed with brine, dried over Na_2SO_4, and the solvent removed by rotary evaporation. The product was isolated by flash chromatography on silica gel using 20:80 ethyl acetate-hexane as eluant. The product (0.5902 g, 2.324 mmoles, 26.49%) was a clear yellow oil. ^{1}H NMR ($CDCl_3$, 500 MHz): δ 6.93 (m, ^3J = 15.7 Hz, ^4J = 6.9 Hz, 2H), 5.81 (m, ^3J = 15.7 Hz, ^4J = 1.5 Hz, 2H), 4.18 (q, J = 7.1 Hz, 4H), 2.21 (m, 4H), 1.49 (m, 4H), 1.28 (t, J = 7.0 Hz, 6H); ^{13}C NMR ($CDCl_3$, 125 MHz): δ 166.63 (2C), 148.58 (2CH), 121.67 (2CH), 60.19 ($2CH_2$), 31.87 ($2CH_2$), 27.48 ($2CH_2$), 14.27 ($2CH_3$); IR (neat): 2981.71, 2935.79, 2861.47, 1721.36, 1655.01, 1368.23, 1267.23, 1182.52, 1044.85 cm^{-1}; MS: *m/z* 254.2, 180.2, 135.1, 107.1, 81.1, 67.1, 55.1; R_f: 0.31 (20:80 EtOAc-hexane, visualized with $KMnO_4$ stain). ^{1}H NMR, ^{13}C NMR, IR, and MS data matched literature values.[18]

*Synthesis of Cyclohexane-1,2-diacetic acid diethyl ester (**17** and **18**).*— The bulk electrolysis conditions described above were used for each reaction. Deca-2,8-dienedioic acid diethyl ester (**3**) was used as the EHC substrate. ^{1}H NMR ($CDCl_3$, 500 MHz): (*mixture of cis and trans*): δ 4.12 (q, J = 7.1 Hz, 8H), 2.48 (dd, ^2J = 14.8 Hz, ^3J = 3.8 Hz, 2H, *trans*), 2.24 (m, 3H, *cis*), 2.19 (m, 2H, *cis*), 2.09 (dd, ^2J = 14.8 Hz, ^3J = 8.4, 2H, *trans*), 1.75 (m, 3H, *trans*), 1.68 (m, 3H, *trans*), 1.57 (m, 11H), 1.25 (t, ^3J = 7.1, 13H); ^{13}C NMR ($CDCl_3$, 125 MHz): (*cis isomer*): δ 173.21 (2C), 60.29 ($2CH_2$), 35.75 (2CH), 35.55 ($2CH_2$), 28.81 ($2CH_2$), 23.84 ($2CH_2$), 13.55 ($2CH_3$); (*trans isomer*): δ 173.17 (2C), 60.26 ($2CH_2$), 39.28 (2CH), 39.09 ($2CH_2$), 32.36 ($2CH_2$), 25.80 ($2CH_2$), 14.26 ($2CH_3$); IR (neat): 2981.33, 2929.77, 2856.46, 1733.16, 1439.25, 1340.52 cm^{-1}; MS: *m/z* 211.2, 169.2, 165.1, 123.1, 95.1, 81.1. ^{1}H NMR, ^{13}C NMR, IR, and MS data matched literature values for the *cis* and *trans* isomers.[20]

Results and Discussion

Computational studies.— The mechanism of electron transfer between reduced metal-salen and substrate was examined using computational chemistry methods. Metal-salens investigated included Ni(II)-, Zn(II)-, Co(II)-, and Cu(II)-salen, while substrates studied were the electron-deficient alkenes acrylonitrile and methyl acrylate. Using density functional theory (DFT) calculations carried out with the Gaussian03 quantum chemistry program,[21] the overall energy for the electron transfer reaction (ΔG°, eqn 1) between each reduced metal-salen and each substrate was determined.

$$[\mathrm{M(II)-salen}]^- + \mathrm{substrate} \rightarrow \mathrm{M(II)-salen} + [\mathrm{substrate}]^- \quad [1]$$

The activation energy for electron transfer ($\Delta G^{\dagger}_{et}$) via an outer sphere (OS) mechanism was calculated according to Marcus Theory[22] (eqn 2), where is λ is the reorganization energy and ΔG° is again the overall energy for

$$\Delta G^{\dagger}_{et} = \frac{(\Delta G^{\circ} + \lambda)^2}{4\lambda} \quad [2]$$

the electron transfer reaction. The reorganization energy λ is the sum of both the internal reorganization energy of the acceptor and donor (λ_i) and the solvent reorganization energy (λ_0). The internal reorganization energy λ_i is given by eqn 3, where $\mathrm{E}\left([\mathrm{M(II)-salen}]^-; \mathrm{M(II)-salen}\right)$ is the electronic energy of the reduced metal-salen at the

$$\begin{aligned}\lambda_i = \{&\mathrm{E}([\mathrm{M(II)-salen}]^-; \mathrm{M(II)-salen}) \\ &+ \mathrm{E}(\mathrm{substrate}; [\mathrm{substrate}]^-)\} \\ &- \{\mathrm{E}([\mathrm{M(II)-salen}]^-; [\mathrm{M(II)-salen}]^-) \\ &+ \mathrm{E}(\mathrm{substrate}; \mathrm{substrate})\}\end{aligned} \quad [3]$$

equilibrium geometry of the neutral metal-salen, E(substrate; $[\mathrm{substrate}]^-$) is the electronic energy of the neutral substrate at the equilibrium geometry of the reduced substrate, and $\mathrm{E}\left([\mathrm{M(II)-salen}]^-; [\mathrm{M(II)-salen}]^-\right)$ and E (substrate; substrate) are the electronic energies of the reduced metal-salen and neutral substrate at their equilibrium geometries. The solvent reorganization energy λ_0 is given by eqn 4, where

$$\lambda_0 = \frac{(\Delta e)^2}{4\pi\varepsilon_0}\left(\frac{1}{2r_A} + \frac{1}{2r_B} - \frac{1}{R}\right)\left(\frac{1}{\varepsilon_\infty} - \frac{1}{\varepsilon_r}\right) \quad [4]$$

r_A is the radius of the reduced metal-salen, r_B is the radius of the neutral substrate, R is the distance between the reduced metal-salen and neutral substrate at the point of electron transfer, ε_0 is the permittivity of vacuum (8.854 * 10^{-12} C^2/J*m), ε_∞ is the fast dielectric constant of the solvent (equal to the square of the index of refraction), ε_r is the bulk dielectric constant of the solvent, and Δe is the amount of charge transferred (in this case, 1 e^- = 1.602 * 10^{-19} C). For acetonitrile solvent, ε_∞ = 1.80 and ε_r = 37.5 at 25°C.[23] The radii r_A and r_B were computed using the volume calculated in Gaussian for the equilibrium geometries and the assumption that the molecules were spherical. Distance R was taken to be the sum of radii r_A and r_B.

The activation energy for electron transfer via an inner sphere (IS) mechanism was calculated using the free energy difference between reduced metal-salen and substrate reactants and the transition state for carbon-carbon bond formation between the ligand of the reduced metal-salen and the substrate (Figure 2). The relative free energy of the intermediate is similarly computed as the free energy difference between reduced metal-salen and substrate reactants and the intermediate structure resulting from the carbon-carbon bond formation.

All DFT calculations utilized the B97-1 functional,[24,25] which was previously demonstrated to optimally reproduce crystal structures and experimental electron affinities for Ni(II)-salens[13] and has

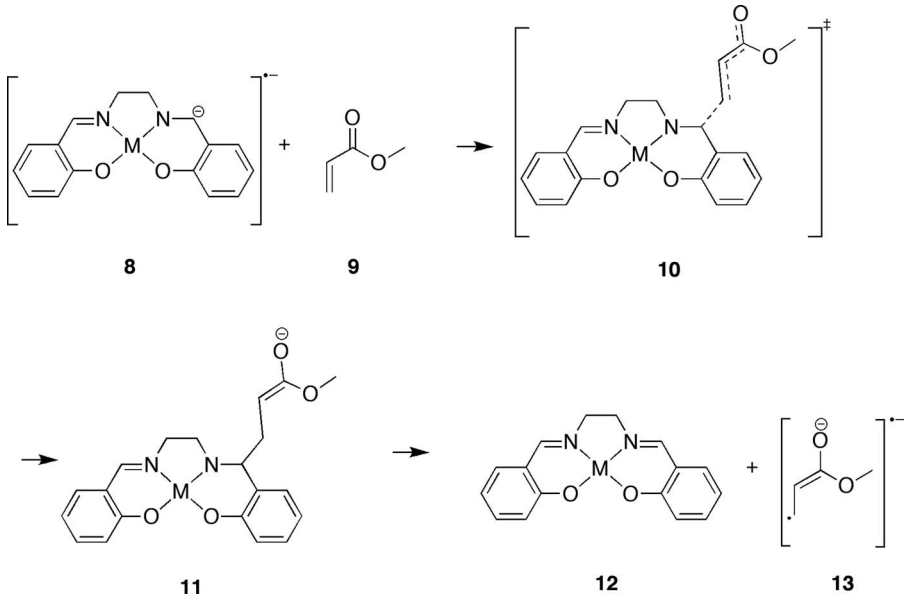

Figure 2. Mechanism for IS electron transfer, illustrating the transition state and intermediate formed in the case of methyl acrylate as the substrate and carbon-carbon bond formation occurring at the β-carbon of the substrate.

also been shown to perform well for the prediction of 3d transition metal thermochemistry.[26] Geometries were optimized using the 6-31G(d,p) basis set for all atoms, except for the metals for which the Stuttgart effective core potential basis set was used.[27] Final electronic energies were calculated using the optimized geometries and the 6-311++G(d,p) basis set on all atoms, except for the metals for which the Stuttgart effective core potential basis set was used. Stationary points were verified as minima or transition states using vibrational frequency calculations, which also allowed for free energies to be calculated. Solvation energies in acetonitrile solvent were obtained using the IEF-PCM (implicit solvation using the polarizable continuum model with the integral equation formalism)[28] method as implemented in Gaussian03. In computing activation free energies for the transition states and intermediates involved in the IS pathway, a translational entropy correction was included so as to account for the difference in standard state concentrations in the gas phase (1/24.5 M based upon standard pressure of 1 atm and the ideal gas law) and in solution (1 M).[29] Percent contribution of an atom's basis functions to a molecular orbital was determined based upon the sum of the square of the coefficients of those basis functions in that molecular orbital.

Adiabatic reduction and oxidation potentials were calculated using free-energy cycles (Scheme 1). The free energy for oxidation and reduction in solution is

$$\Delta G_{ox} = G_g^{X^+} - G_g^X + \Delta G_{sol}^{X^+} - \Delta G_{sol}^X$$
$$\Delta G_{red} = G_g^{X^-} - G_g^X + \Delta G_{sol}^{X^-} - \Delta G_{sol}^X \quad [5]$$

where $G_g^{X^+}$, G_g^X, and $G_g^{X^-}$ are the gas phase energies for the oxidized, originating, and reduced species, and $\Delta G_{sol}^{X^+}$, ΔG_{sol}^X, and $\Delta G_{sol}^{X^-}$ are the corresponding solvation energies. The absolute reduction or oxidation potential is then given according to eqn 6, where F is the Faraday constant and n is the number of electrons transferred. Redox

$$E^\circ = -\frac{\Delta G_{(ox\ or\ red)}}{nF} \quad [6]$$

potentials relative to the standard hydrogen electrode (SHE) are obtained by adding 4.28 V to E° from eqn 6 in the case of oxidation and subtracting 4.28 V from E° from eqn 6 in the case of reduction.[30]

The Fukui nucleophilicity index of an atom was determined from the N-electron equilibrium geometry, and using the difference in Mulliken charge populations for the atom in the N-electron and (N-1)-electron cases.[31] Similarly, the Fukui electrophilicity index of an atom was determined from the N-electron equilibrium geometry, and using the difference in Mulliken charge populations for the atom in the

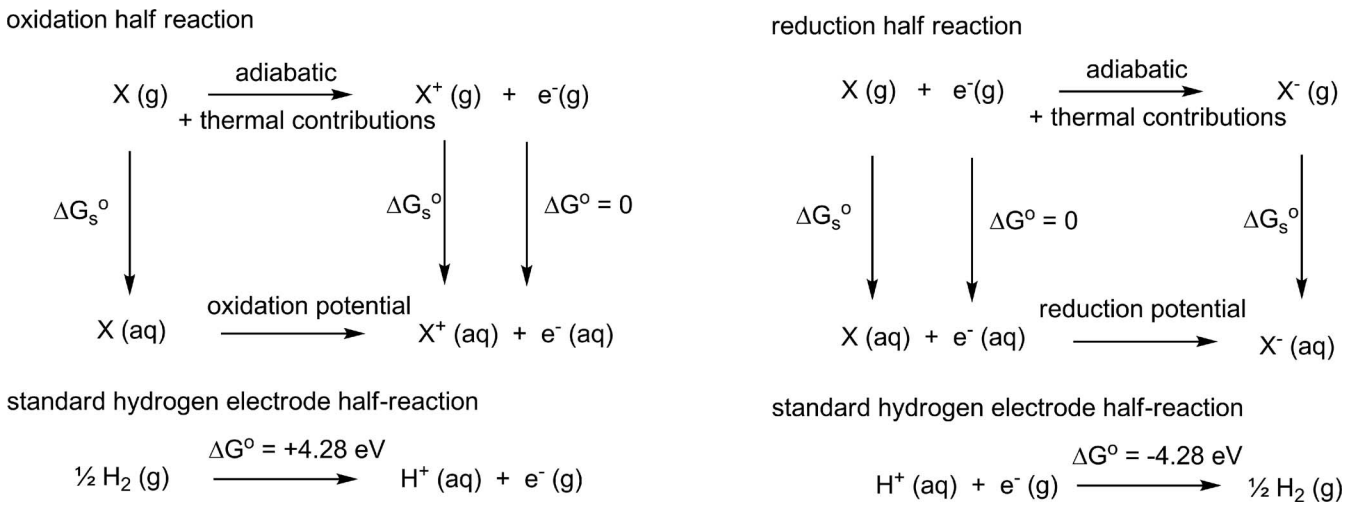

Scheme 1. Free-energy cycles used for calculating adiabatic redox potentials.

Table I. ΔG° (25°C; kcal/mol) for electron transfer from reduced metal-salen to substrate and oxidation potential of the reduced metal-salens (25°C; V; relative to the standard hydrogen electrode).

	methyl acrylate	acrylonitrile	oxidation potential of reduced metal-salen
Ni(II)-salen	−0.76	−3.01	1.96
Zn(II)-salen	−1.91	−4.16	2.01
Co(II)-salen	8.75	6.50	1.55
Cu(II)-salen	13.93	11.68	1.32

(N+1)-electron and (N)-electron cases.[31] The Mulliken charge populations were determined with the more balanced 6-31G(d,p) basis set (except again using the Stuttgart effect core potential basis set for the metals), which was used in the geometry optimizations and which has been shown to be suitable for this purpose in related studies.[32,33]

Computational results/discussion.—Metal-salen spin states.—For the neutral Co(II)-salen, with a d^7 electron configuration for the metal, both doublet and quartet spin states were considered. Likewise, for one-electron reduced Co(II)-salen (giving a d^8 metal center), both singlet and triplet states were computed. For transition states and intermediates along the IS pathway with Co(II)-salen, both open-shell singlet and triplet states were considered. Comparing the relative free energies of the different spin states (Table S1) shows that the lowest energy states for the neutral Co(II)-salen, reduced Co(II)-salen, and Co(II)-salen IS pathway species are the quartet, triplet, and open-shell singlet, respectively. These lowest energy species are then used exclusively in all further calculations involving Co(II)-salen.

For neutral Zn(II)-salen, with a d^{10} configuration, only the singlet spin state was relevant, while reduced species involving Zn were all doublets. The reverse was true for neutral Cu(II)-salen, which has a d^9 configuration and is a doublet, while reduced Cu(II)-salen was a singlet and Cu(II)-salen IS pathway species were open-shell singlets. Given the nearly square planar coordination geometry in Ni(II)-salen, neutral Ni(II)-salen was treated as a singlet, while reduced species involving Ni were all doublets.

Overall thermodynamics of electron transfer.— ΔG° values for the overall electron transfer reaction from reduced metal-salen to neutral substrate are shown in Table I. The order of thermodynamic favorability for the electron transfer by metal center (regardless of substrate) was found to be Zn(II) > Ni(II) » Co(II) > Cu(II). This order was consistent with computed oxidation potentials for the reduced metal-salens, in which the oxidation potentials for reduced Zn(II)- and Ni(II)-salen were found to be ∼0.55 V higher than for reduced Co(II)- and Cu(II)-salen. The more positive potentials for the reduced Zn(II)- and Ni(II)-salen cases correlate with a more thermodynamically favorable oxidation according to the Nernst equation in which ΔG° ∝ -E°. The computed reduction potentials for methyl acrylate (−1.93 V) and acrylonitrile (−1.83 V) indicate a 0.1 V preference for the reduction of acrylonitrile and support the lower ΔG° values for electron transfer with acrylonitrile as the substrate.

Table III. Fukui electrophilicity index of the α- and β-carbons in the substrates.

	α-carbon	β-carbon
methyl acrylate	0.047	0.120
acrylonitrile	0.110	0.140

Kinetics and mechanism of electron transfer.— In first examining the IS electron transfer pathway, carbon-carbon bond formation between the imine carbon of the metal-salen and the substrate could occur at either the α-carbon or β-carbon of the alkene group in methyl acrylate and acrylonitrile. Comparing the activation energies ($\Delta G^{\dagger}_{et}$) and energies of the IS intermediates relative to reactants (ΔG^{o}_{int}) in the gas phase shows a clear energetic preference for the IS pathway at the β-carbon of the substrate (Table II). Both gas phase $\Delta G^{\dagger}_{et}$ and ΔG^{o}_{int} are ∼16-17 kcal/mol lower for methyl acrylate and ∼14-15 kcal/mol lower for acrylonitrile when the IS pathway proceeds through the substrate β-carbon. The IS pathway can be considered a reaction between the nucleophilic imine carbon on the metal-salen and the electrophilic substrate. The higher Fukui electrophilicity index for the substrate β-carbons versus the α-carbons (Table III) thus supports the preferred IS reactivity at the substrate β-carbon. Given these results, all further discussion of the IS pathway will refer only to reaction at the substrate β-carbon.

Within the IS pathway via the β-carbon of the substrate (Table II), kinetic preference for electron transfer followed in the order Ni(II) > Zn(II) » Co(II) » Cu(II). Viewing the IS reaction as occurring between the nucleophilic carbanion and the electrophilic substrate, the computed Fukui nucleophilicities[31] for the anionic carbon in the reduced metal-salens (Table IV) show the Ni(II) and Zn(II) cases to be more nucleophilic and therefore more reactive than the Co(II) and Cu(II) cases.

More importantly, it may be observed that the IS pathway relies on the presence of the formal carbanion at the imine carbon on the ligand of the reduced metal-salen (Figure 2), and therefore on the reduction of the neutral metal-salen being ligand-based as opposed to metal-based. The minimal change in charge at the metal center upon reduction of Ni(II)-salen and Zn(II)-salen (Table IV) suggests that reduction is occurring primarily on the salen ligand in these cases. In contrast,

Table II. IS pathway thermodynamics (25°C; kcal/mol) with bond formation at the α-carbon and β-carbon of (a) methyl acrylate and (b) acrylonitrile substrates.

	α-carbon, gas phase		β-carbon, gas phase		β-carbon, solution	
(a)	$\Delta G^{\dagger}_{et}$	ΔG^{o}_{int}	$\Delta G^{\dagger}_{et}$	ΔG^{o}_{int}	$\Delta G^{\dagger}_{et}$	ΔG^{o}_{int}
Ni(II)-salen	24.05	24.11	6.62	6.42	11.59	11.10
Zn(II)-salen	25.58	25.72	9.16	9.16	12.91	12.79
Co(II)-salen	32.48	32.44	16.01	15.32	21.01	19.87
Cu(II)-salen	38.91	38.67	22.08	21.78	28.90	28.43
	α-carbon, gas phase		β-carbon, gas phase		β-carbon, solution	
(b)	$\Delta G^{\dagger}_{et}$	ΔG^{o}_{int}	$\Delta G^{\dagger}_{et}$	ΔG^{o}_{int}	$\Delta G^{\dagger}_{et}$	ΔG^{o}_{int}
Ni(II)-salen	16.76	17.33	3.05	1.64	7.74	7.02
Zn(II)-salen	18.59	19.22	5.00	3.42	8.34	7.97
Co(II)-salen	25.66	25.84	12.20	10.64	17.00	16.28
Cu(II)-salen	31.88	31.46	18.21	16.72	24.95	23.47

Table IV. Electronic characterization of the reduced metal-salens.

	% metal character in LUMO of neutral metal-salen	change in Mulliken charge for metal upon reduction of neutral metal-salen	change in metal-N and metal-O bond length upon reduction (Å)	Fukui nucleophilicity index of anionic carbon in reduced metal-salen
Ni(II)-salen	4.61%	−0.090	−0.005, +0.022	0.065
Zn(II)-salen	0.95%	−0.078	−0.029, +0.021	0.061
Co(II)-salen	45.57%	−0.244	−0.056, +0.049	0.058
Cu(II)-salen	59.36%	−0.387	+0.168, +0.140	0.030

the Mulliken charge of the cobalt and copper centers in those metal-salens decreases by 3-4 times as much as occurs with nickel and zinc. The greater participation of the metal center in the reduction process in Co(II)-salen and Cu(II)-salen is further shown by the significant degree of metal character in the LUMO of the neutral metal-salens (Table IV). The nominal degree to which the metal contributes to the LUMO in Ni(II)-salen and Zn(II)-salen explains the small change in charge at those metal centers upon reduction. Visualization of the LUMOs for the neutral metal-salens (Figure 3) further emphasizes the ligand-based reduction occurring with Ni(II)-salen and Zn(II)-salen, which facilitates the IS pathway, and the largely metal-based reduction occurring with Co(II)-salen and Cu(II)-salen. Additional support of the ligand-based reduction occurring in Ni(II)-salen and Zn(II)-salen is provided by the very small changes in the metal-N and metal-O bond lengths upon reduction (Table IV), consistent with little to no participation of the metal in the LUMO of the neutral metal-salen. As the metal-based character of the LUMO increases in going to Co(II)-salen and Cu(II)-salen, progressively larger changes in the metal-N and metal-O bond lengths are observed upon reduction. In particular, for Cu(II)-salen, where reduction is to the largest degree metal-based, a significant increase of 0.140 Å and 0.168 Å is seen for the Cu-N and Cu-O bond lengths, respectively, which is consistent with occupation of the Cu(II)-salen LUMO shown in Figure 3 exhibiting antibonding d character.

Contrary to the results obtained here, previous computations on neutral and reduced Ni(II)-salen and imino substituted Ni(II)-salens had suggested that the LUMO of the neutral Ni(II)-salen was metal-centered, with a low-lying ligand-based LUMO+1 molecular orbital (2-3 kcal/mol higher in energy for Ni(II)-salen).[10,11] Further examination of the Ni(II)-salen orbitals in the present work reveals that the LUMO+1 is low-lying (2.84 kcal/mol above the LUMO) and even more ligand-based than the LUMO. The first metal-based orbital is the LUMO+2 at 16.73 kcal/mol above the LUMO; given this large energy gap, it is unlikely for this metal-based orbital to play any role in the reduction of Ni(II)-salen. It is worth noting that the ligand-based reduction of Ni(II)-salen shown here is consistent with the ligand-based reactivities observed experimentally with Ni(II)-salen.[6,9]

Table V. Activation energy for the OS pathway (25°C; kcal/mol) with methyl acrylate and acrylonitrile substrates.

	methyl acrylate	acrylonitrile
Ni(II)-salen	9.20	7.87
Zn(II)-salen	8.53	7.44
Co(II)-salen	14.39	13.00
Cu(II)-salen	20.35	18.89

Within the OS pathway, kinetic preference for electron transfer followed in the order Zn(II) > Ni(II) » Co(II) > Cu(II) (Table V). As the OS pathway relies on the ability of the reduced metal-salen to transfer away an electron to the substrate, the trend here correlates with reduced Zn(II)-salen and Ni(II)-salen having oxidation potentials approximately 0.55 V higher than for reduced Co(II)-salen and Cu(II)-salen (Table I). The slightly lower OS activation energies with Zn(II)-salen concur with the slightly higher oxidation potential for reduced Zn(II)-salen versus reduced Ni(II)-salen (by 0.05 V). Further, the lower OS activation energies with acrylonitrile compared to methyl acrylate can be attributed to the 0.10 V preference for the reduction of the former compared to the latter.

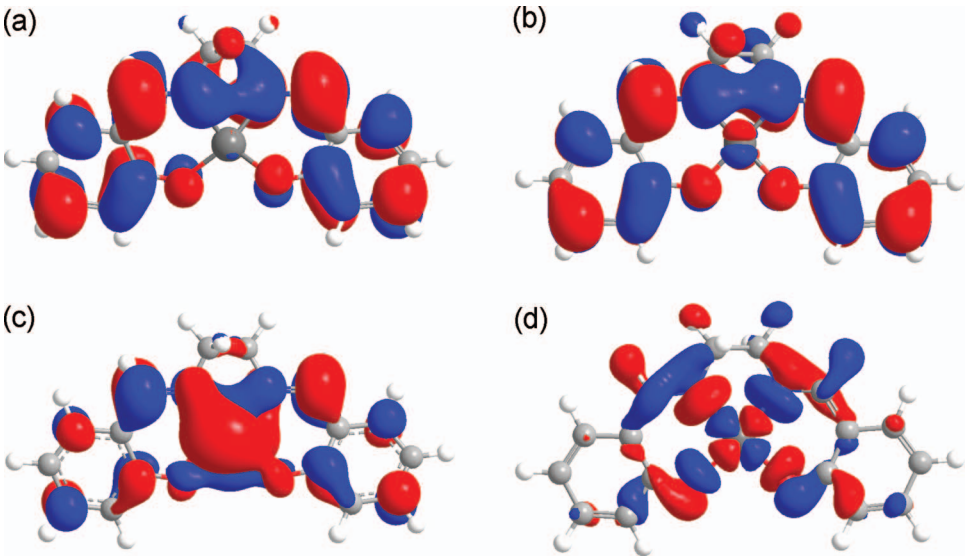

Figure 3. LUMO of the neutral metal-salens. (a) Zn(II)-salen, (b) Ni(II)-salen, (c) Co(II)-salen, (d) Cu(II)-salen.

Table VI. $\Delta\Delta G^{\dagger}_{et}$(25°C; kcal/mol) for OS pathway versus IS pathway (β-carbon) with methyl acrylate and acrylonitrile substrates.

	methyl acrylate	acrylonitrile
Ni(II)-salen	−2.39	+0.13
Zn(II)-salen	−4.39	−0.90
Co(II)-salen	−6.62	−4.00
Cu(II)-salen	−8.55	−6.06

The competing IS and OS electron transfer pathways can be assessed by examining the difference in $\Delta G^{\dagger}_{et}(\Delta\Delta G^{\dagger}_{et} = \Delta G^{\dagger}_{et}(OS) - \Delta G^{\dagger}_{et}(IS))$ between the two pathways (Table VI). Activation energies for electron transfer were generally lower for the outer sphere pathway (with the only exception being Ni(II)-salen with acrylonitrile being ∼0.1 kcal/mol higher for the outer sphere pathway). Preference for OS versus IS electron transfer is smallest with Ni(II) and Zn(II), in which cases reduction of the metal-salen is most ligand-based and IS electron transfer is relatively facile. On the other hand, the difference in $\Delta G^{\dagger}_{et}$ between OS and IS pathways is greatest with Co(II) and Cu(II), in which cases reduction of the metal-salen is most metal-based and IS electron transfer is strongly disfavored.

Implications for ERC and EHC reactions.— The computational results suggest that Ni(II)-salen and Zn(II)-salen are superior choices for a metal-salen to serve as an electrocatalyst to facilitate electron transfer to the substrate. The barrier for IS electron transfer with these two metal-salens is ∼8.5 kcal/mol lower than with Co(II) and ∼16.5 kcal/mol lower than with Cu(II); the barrier for OS electron transfer, ∼5.5 kcal/mol lower than with Co(II) and ∼11 kcal/mol lower than with Cu(II).

The data further suggest potential advantages of using either Ni(II)-salen or Zn(II)-salen as the electrocatalyst. $\Delta\Delta G^{\dagger}_{et}$ between OS and IS pathways is larger for Zn(II)-salen versus Ni(II)-salen by ∼1 kcal/mol with acrylonitrile and ∼2 kcal/mol with methyl acrylate as the substrate (cf. Table VI). In addition, the IS pathway barriers are ∼0.8–1.5 kcal/mol lower with Ni(II)-salen versus Zn(II)-salen (cf. Table II). Thus, while both Ni(II)-salen and Zn(II)-salen would be effective electrocatalysts, Zn(II)-salen would tend toward the OS pathway. Ni(II)-salen, on the other hand, would be more likely to promote IS electron transfer, which in turn can allow for the possibility of post-electron transfer reactivity (i.e., in an EHC or ERC reaction) of the reduced substrate to occur while still bound to the metal-salen via the covalent bond to the imine carbon of the salen ligand. Ni(II)-salen would then be the optimal choice of metal-salen among those considered in this study to allow for the metal-salen structure to potentially induce stereoselectivity into EHC and ERC reaction processes.

Cyclic Voltammetry (CV).— In order to investigate the mechanism of the mediated EHC reaction, we elected to study the various Ni(II)-salen compounds shown in Figure 4. These compounds include the parent Ni(II)-salen **4**, the chiral (R,R) Ni(II)-salen **5**, and the chiral (S,S) Ni(II)-salen **6**. The cyclic voltammetry results of the various Ni(II)-salen compounds in the presence of EHC substrate **3** are shown in Figures 5, 6, and 7. The cyclic voltammetry results of EHC substrate **3** are shown in Figure 8.

Figure 8 showed that the EHC substrate exhibits an irreversible curve at −2.3 V. Each Ni(II)-salen compound exhibits a one-electron, reversible curve. Each Ni(II)-salen compound shows the presence of a significant amount of catalytic current in the presence of substrate **3**. Observation of the catalytic current indicated that the substrate undergoes an irreversible reaction after reaction with the reduced catalyst.

Bulk electrolysis.— Bode, Sowell, and Little reported the electrolyte-assisted stereoselection and control of cyclization in ERC reactions in 1990.[34] The key factors were the nature of the electrophore and the choice of the supporting electrolyte. Felton and Bauld reported a similar effect of the electrolyte cation on the selectivity of ERC reactions of bis(enones).[35] The authors found that formation of *cis* vs. *trans* cyclobutanes was strongly favored by using magnesium ions, presumably by a chelation effect. Additives can also influence *cis*/*trans* ratio in EHC reactions. Moens, Baizer, and Little reported that the addition of 1.3 equivalents of cerium trichloride resulted in a cyclized *cis*/*trans* ratio of 1:15.[5] When the reaction is run in the absence of cerium trichloride the resulting *cis*/*trans* ratio was 1:7.5. The authors presumed that along the reaction coordinate a complex between the cerium trichloride and substrate formed. It was this complex that was responsible for the increase in *trans* selectivity. Dunach has used chiral metal salen complexes in mediated intramolecular reductive cyclizations.[36] In the cyclization of citronellyl bromide, *p*-menthane was made with a *trans*/*cis* ratio of 1.0:0.9.

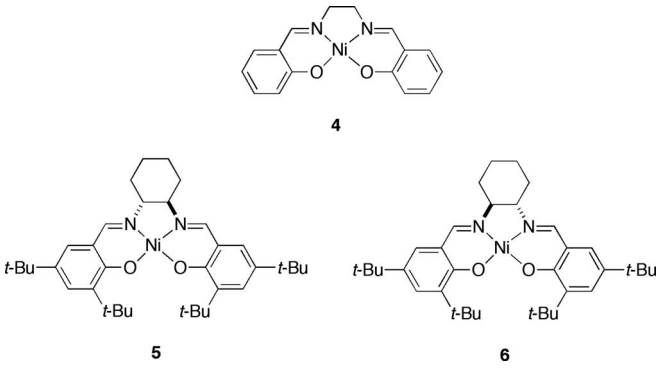

Figure 4. Ni(II)-salen **4** and chiral Ni(II)-salen derivatives **5** and **6**.

As shown in Scheme 2, the possibility exists to control the absolute stereochemistry of the EHC reaction by using a C_2 symmetric ligand. For example, using C_2 symmetric catalyst **4** in an EHC reaction implies the existence of intermediate **14**. If in intermediate **15**, the cyclization step occurred concertedly with reduction of the salen moiety and scission of the bond linking the catalyst and the substrate, then the possibility exists to perhaps affect which diastereotopic face of alkene is attacked. The chirality in the ligand could be transmitted to which diastereotopic face of the alkene is attacked in the cyclization step.

In order to explore the effectiveness of the Ni(II)-salens shown above in mediated EHC reactions, we elected to perform bulk electrolysis reactions using EHC substrate **3** that would result in either *cis* cyclized diastereomer **17** or *trans* diastereomer **18**. The overall reaction is shown in Scheme 3. The reactions were performed at a reduction potential that ensured that the EHC substrate was not being directly reduced. The results of these experiments are summarized in Table VII.

The results indicate that both chiral Ni(II)-salens are effective mediators in the EHC reaction. The parent Ni(II)-salen was shown to give the highest amount of *trans* cyclized product. Both chiral Ni(II)-salen catalysts gave lower selectivity and lower yields. This may indicate that the increased steric bulk of the substituents around the salen ligand lowers the reactivity of the catalyst when compared to an unsubstituted Ni(II)-salen.

Table VII. Bulk Electrolysis (BE) reactions of Ni(II)-salens with EHC substrate 3.

	Reaction yield (%)	*cis*/*trans ratio*
Ni(II)-salen 4	95.0	1/1.46
(R,R) Ni(II)-salen 5	73.8	1/1.20
(S,S) Ni(II)-salen 6	67.0	1/1.31

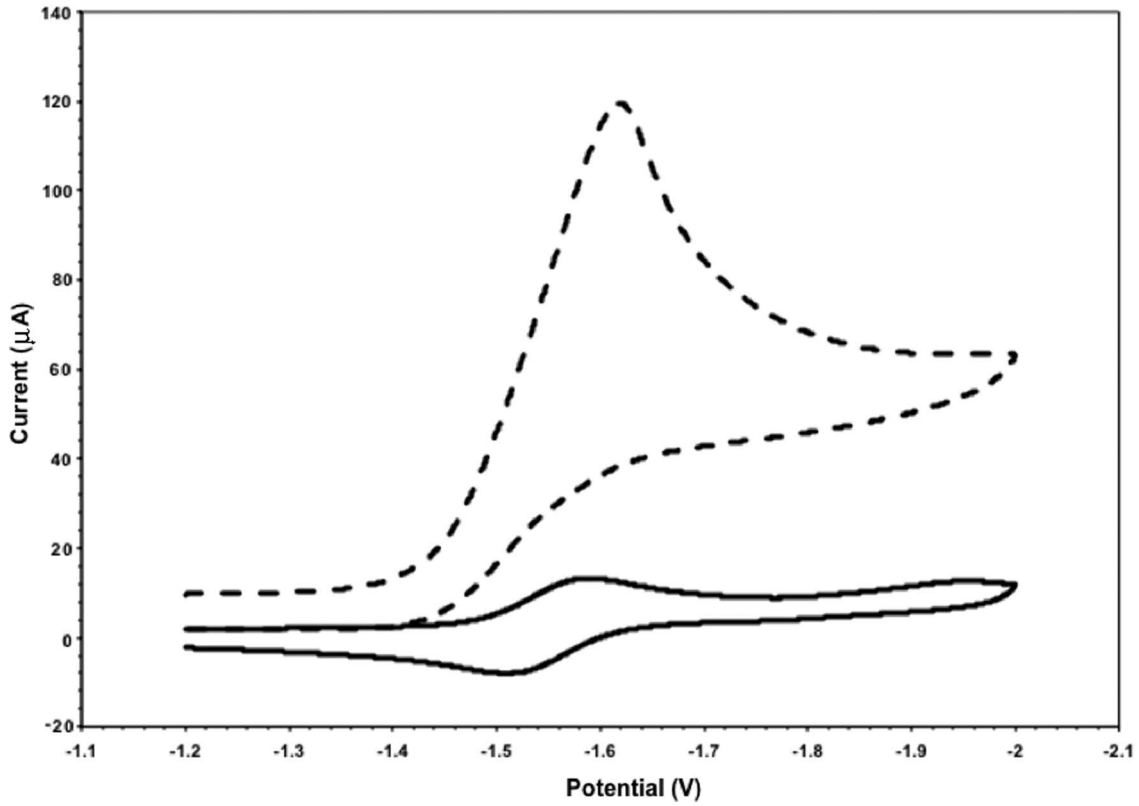

Figure 5. Cyclic voltammetry of 1 mM Ni(II)-salen **4** (solid line) in DMF and 1 mM Ni(II)-salen **4** with 10 mM EHC substrate **3** (dashed line) in DMF. Scan rate = 0.1 V/sec.

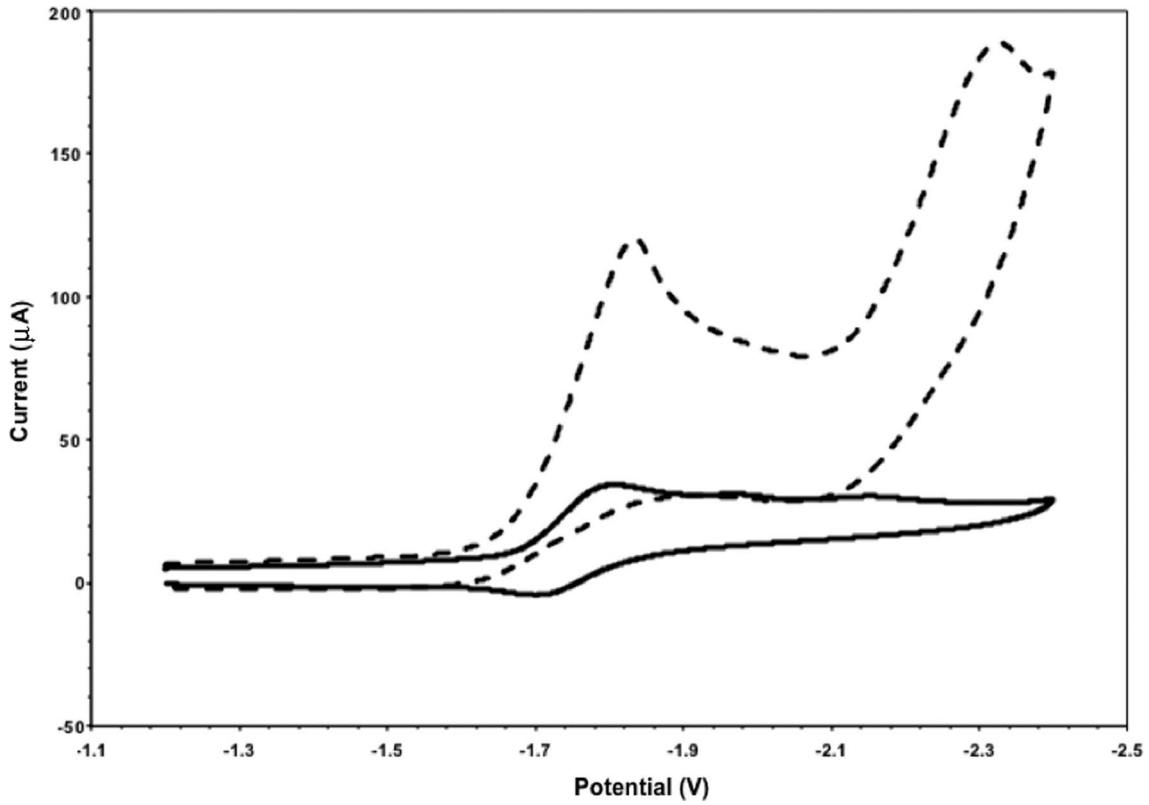

Figure 6. Cyclic voltammetry of 1 mM (R,R) Ni(II)-salen **5** (solid line) in DMF and 1 mM (R,R) Ni(II)-salen **5** with 10 mM EHC substrate **3** (dashed line) in DMF. Scan rate = 0.1 V/sec.

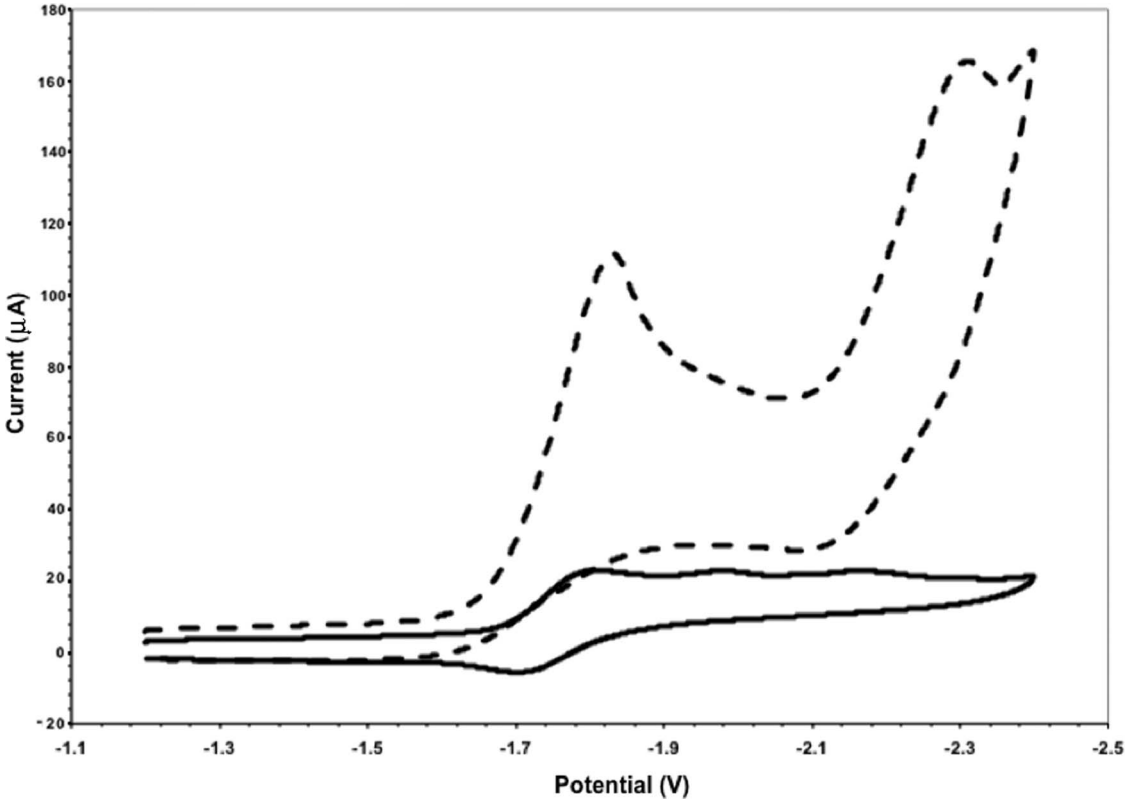

Figure 7. Cyclic voltammetry of 1 mM (S,S) Ni(II)-salen **6** (solid line) in DMF and 1 mM (S,S) Ni(II)-salen **6** with 10 mM EHC substrate **3** (dashed line) in DMF. Scan rate = 0.1 V/sec.

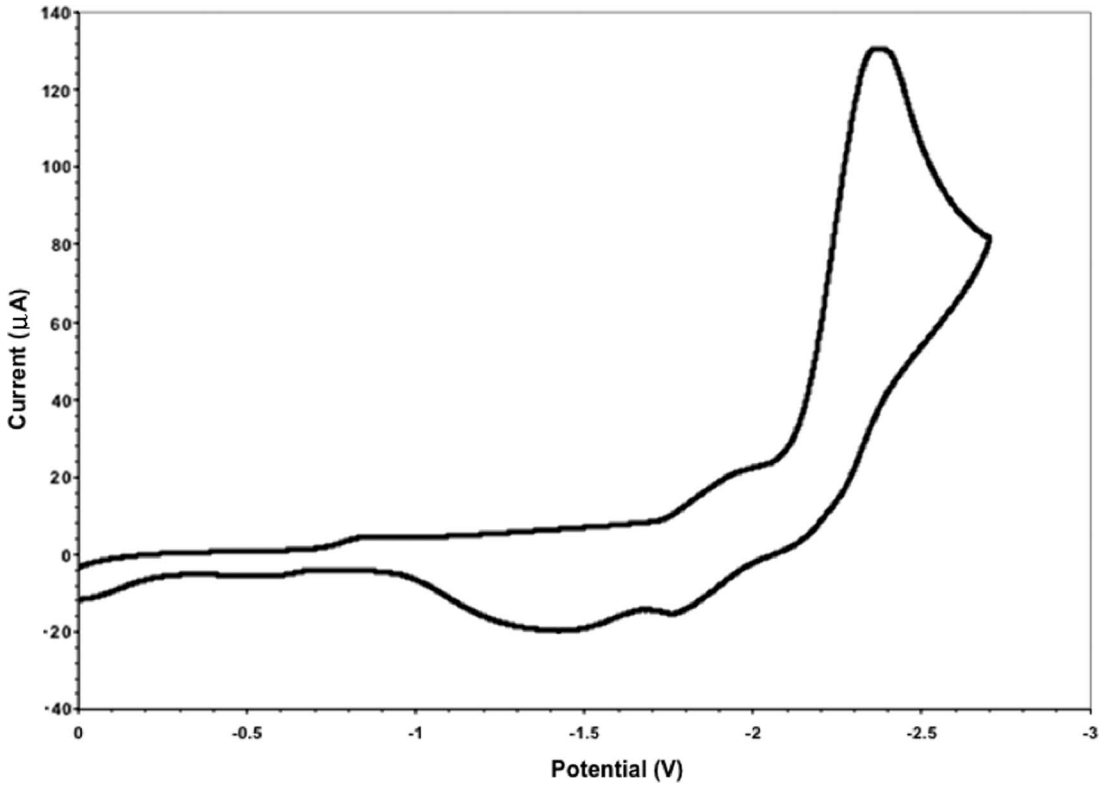

Figure 8. Cyclic voltammetry of 10 mM EHC substrate **3** in DMF. Scan rate = 0.1 V/sec.

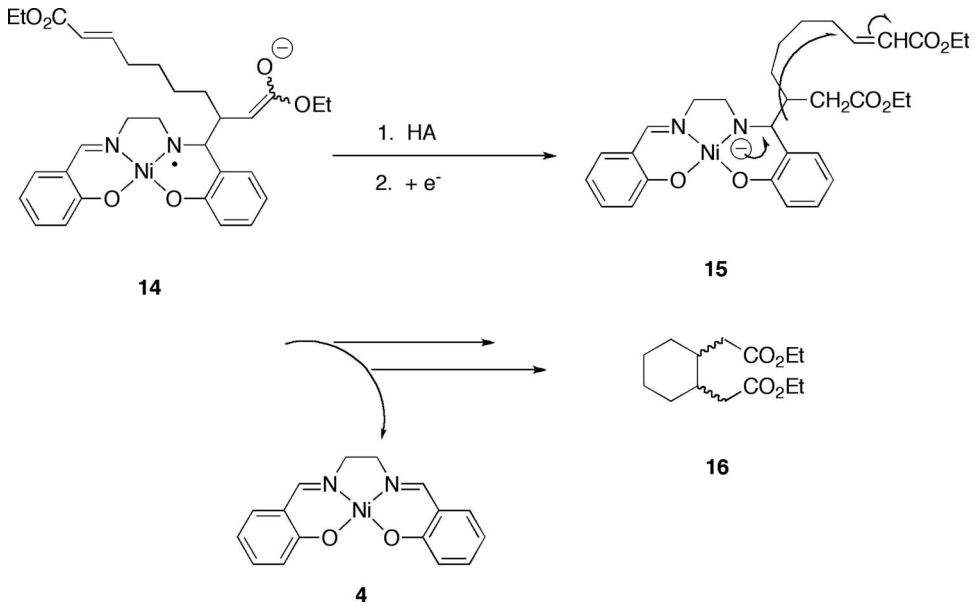

Scheme 2. Control of stereochemistry using a C_2 symmetric ligand.

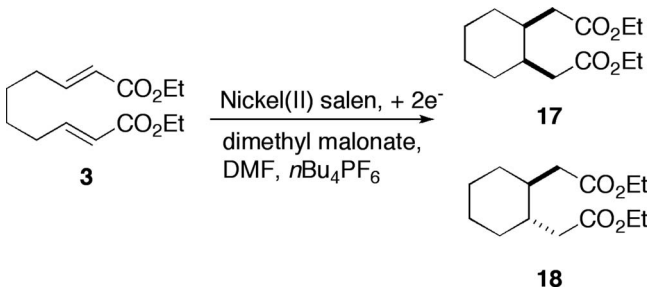

Scheme 3. Mediated electrohydrocyclization (EHC) reactions using Ni(II)-salen derivatives.

Conclusions

Computational chemistry showed that electron transfer from various reduced metal-salens to both methyl acrylate and acrylonitrile was most thermodynamically favored with the Zn(II) and Ni(II) metal centers, while the free energies for electron transfer were considerably higher with the Co(II) and Cu(II) metal centers. Reduced Zn(II)- and Ni(II)-salen also had significantly lower activation energies for electron transfer along both the inner sphere (attributed to ligand-centered reduction of the neutral Zn(II)- and Ni(II)-salens) and outer sphere pathways (attributed to the higher oxidation potentials of the reduced Zn(II)- and Ni(II)-salens). Computational data suggested that, between Zn(II)- and Ni(II)-salen, the latter was more likely to promote IS electron transfer and create the opportunity to impart stereoselectivity into mediated EHC and ERC reactions.

Cyclic voltammetry established the existence of a catalytic current with Ni(II)-salen **4** and chiral Ni(II)-salens **5** and **6** when using EHC substrate **3**. Both chiral Ni(II)-salen catalysts proved to be effective electron transfer agents in mediated EHC reactions from bulk electrolysis. The diastereoselectivity of the cyclization always favored the *trans* product and was lower with the chiral catalysts. This may be due to the increased steric bulk of the chiral ligands preventing conjugate addition of the reduced complex to the EHC substrate.

We are currently investigating other Ni(II)-salen derivatives in mediated EHC reactions. These derivatives include a phenyl ring as a replacement for the ethyl bridge in Ni(II)-salen. We are also interested in investigating the catalytic behavior of Zn(II)-salen in mediated ERC and EHC reactions. The results of these experiments will be reported in due course.

Acknowledgments

We gratefully acknowledge the National Science Foundation for funding this work through a Major Research Instrumentation grant (#0922676). We also thank California State University, Sacramento, College of Natural Science and Mathematics for their support of this research.

References

1. R. D. Little and K. D. Moeller, *Electrochem. Soc. Interface*, **11**, 36 (2002).
2. R. D. Little, D. P. Fox, L. Van Hijfte, R. Dannecker, G. Sowell, R. L. Wolin, L. Moens, and M. M. Baizer, *J. Org. Chem.*, **53**, 2287 (1988).
3. C. G. Sowell, R. L. Wolin, and R. D. Little, *Tetrahedron Lett.*, **31**, 485 (1990).
4. A. J. Fry, R. D. Little, and J. Leonetti, *J. Org. Chem.*, **59**, 5017 (1994).
5. L. Moens, M. M. Baizer, and R. D. Little, *J. Org. Chem.*, **51**, 4497 (1986).
6. J. A. Miranda, C. J. Wade, and R. D. Little, *J. Org. Chem.*, **70**, 8017 (2005).
7. A. J. Fry, *Synthetic Organic Electrochemistry*, Wiley–Interscience, New York (1989).
8. N. L. Weinberg, *Industrial Organic Electrosynthesis*, http://electrochem.cwru.edu/encycl/art-o01-org-ind.htm (accessed February 2013).
9. D. M. Goken, M. A. Ischay, D. G. Peters, J. W. Tomaszewski, J. A. Karty, J. P. Reilly, and M. S. Mubarak, *J. Electrochem. Soc.*, **153**, E71 (2006).
10. P. W. Raess, M. S. Mubarak, M. A. Ischay, M. P. Foley, T. B. Jennermann, K. Raghavachari, and D. G. Peters, *J. Electroanal. Chem.*, **603**, 124 (2007).
11. M. P. Foley, P. Du, K. J. Griffith, J. A. Karty, M. S. Mubarak, K. Raghavachari, and D. G. Peters, *J. Electroanal. Chem.*, **647**, 194 (2010).
12. D. M. Goken, D. G. Peters, J. A. Karty, and J. P. Reilly, *J. Electroanal. Chem.*, **564**, 123 (2004).
13. S. B. Bateni, K. R. England, A. T. Galatti, H. Kaur, V. A. Mendiola, A. R. Mitchell, M. H. Vu, B. F. Gherman, and J. A. Miranda, *Beilstein J. Org. Chem.*, **5**, 82 (2009).
14. L. Meites, *Handbook of Analytical Chemistry*, McGraw Hill, New York (1963).
15. K. A. Jamshid, M. Asadi, and A. H. Kianfar, *J. Coord. Chem.*, **62**, 1187 (2009).
16. C. A. Johnson, S. Sharma, B. Subramaniam, and A. Borovik, *J. Am. Chem. Soc.*, **127**, 9698 (2005).
17. K. Omura and D. Swern *Tetrahedron*, **34**, 1651 (1978).
18. B. C. Hong, H. C. Tseng, and S. H. Chen, *Tetrahedron*, **63**, 2840 (2007).
19. W. S. Wadsworth and W. D. Emmons, *J. Am. Chem. Soc.*, **83**, 1733 (1961).
20. R. Kumareswaran, S. P. Shahi, S. Rani, A. Gupta, K. Madhusudanan, and Y. D. Vankar, *ARKIVOC*, 126 (2002).
21. M. J. Frisch, G. W. Trucks, H. B. Schlegel, G. E. Scuseria, M. A. Robb, J. R. Cheeseman, J. J. A. Montgomery, T. Vreven, K. N. Kudin, J. C. Burant, J. M. Millam, S. S. Iyengar, J. Tomasi, V. Barone, B. Mennucci, M. Cossi, G. Scalmani, N. Rega, G. A. Petersson, H. Nakatsuji, M. Hada, M. Ehara, K. Toyota, R. Fukuda, J. Hasegawa, M. Ishida, T. Nakajima, Y. Honda, O. Kitao, H. Nakai, M. Klene, X. Li, J. E. Knox, H. P. Hratchian, J. B. Cross, V. Bakken, C. Adamo, J. Jaramillo, R. Gomperts, R. E. Stratmann, O. Yazyev, A. J. Austin, R. Cammi, C. Pomelli, J. W. Ochterski, P. Y. Ayala, K. Morokuma, G. A. Voth, P. Salvador,

J. J. Dannenberg, V. G. Zakrzewski, S. Dapprich, A. D. Daniels, M. C. Strain, O. Farkas, D. K. Malick, A. D. Rabuck, K. Raghavachari, J. B. Foresman, J. V. Ortiz, Q. Cui, A. G. Baboul, S. Clifford, J. Cioslowski, B. B. Stefanov, G. Liu, A. Liashenko, P. Piskorz, I. Komaromi, R. L. Martin, D. J. Fox, T. Keith, M. A. Al-Laham, C. Y. Peng, A. Nanayakkara, M. Challacombe, P. M. W. Gill, B. Johnson, W. Chen, M. W. Wong, C. Gonzalez, and J. A. Pople, *Gaussian 03, Revision D.01*, Gaussian, Inc., Wallingford, CT 2004.
22. R. A. Marcus, *Annu. Rev. Phys. Chem.*, **15**, 155 (1964).
23. D. R. Lide, *Handbook of Chemistry and Physics*, 85th Edition, CRC Press, Boca Raton (2004).
24. F. A. Hamprecht, A. J. Cohen, D. J. Tozer, and N. C. Handy, *J. Chem. Phys.*, **109**, 6264 (1998).
25. A. D. Becke, *J. Chem. Phys.*, **107**, 8554 (1997).
26. W. Jiang, M. L. Laury, M. Powell, and A. K. Wilson, *J. Chem. Theory Comput.*, **8**, 4102 (2012).
27. M. Dolg, U. Wedig, H. Stoll, and H. Preuss, *J. Chem. Phys.*, **86**, 866 (1987).
28. J. Tomasi, B. Mennucci, and R. Camini, *Chem. Rev.*, **105**, 2999 (2005).
29. C. J. Cramer, *Essentials of Computational Chemistry: Theories and Models*, 2nd ed., John Wiley & Sons, Ltd., West Sussex, England (2004).
30. C. P. Kelly, C. J. Cramer, and D. G. Truhlar, *J. Phys. Chem. B*, **110**, 16066 (2006).
31. R. G. Parr and W. Yang, *Density Functional Theory of Atoms and Molecules*, Oxford University Press, New York (1989).
32. M. F. Brown and B. F. Gherman, *Theor. Chem. Acc.*, **128**, 137 (2011).
33. N. W. Aboelella, S. V. Kryatov, B. F. Gherman, W. W. Brennessel, V. G. Young, Jr., R. Sarangi, E. V. Rybak-Akimova, K. O. Hodgson, B. Hedman, E. I. Solomon, C. J. Cramer, and W. B. Tolman, *J. Am. Chem. Soc.*, **126**, 16896 (2004).
34. H. E. Bode, C. G. Sowell, and R. D. Little *Tetrahedron Lett.*, **31**, 2525 (1990).
35. A. N. Felton and N. L. Bauld, *Tetrahedron Lett.*, **45**, 8465 (2004).
36. E. Dunach, A. P. Esteves, A. M. Freitas, M. J. Medeiros, and S. Olivero, *Tetrahedron Lett.*, **40**, 8693 (1999).